

# A new statistical test for static stress triggering: Application to the 1987 Superstition Hills earthquake sequence

Greg Anderson and Hadley Johnson

Cecil H. and Ida M. Green Institute of Geophysics and Planetary Physics,  
University of California, San Diego

**Abstract.** Over the past several years, many investigators have argued that static stress changes caused by large earthquakes influence the spatial and temporal distributions of subsequent regional seismicity, with earthquakes occurring preferentially in areas of stress increase and reduced seismicity where stress decreases. Some workers have developed quantitative methods to test for the existence of such static stress triggering, but no firm consensus has yet been reached as to the significance of these effects. We have developed a new test for static stress triggering in which we compute the change in Coulomb stress on the focal mechanism nodal planes of a set of events spanning the occurrence of a large earthquake. We compare the statistical distributions of these stress changes for events before and after the mainshock to decide if we can reject the hypothesis that these distributions are the same. Such rejection would be evidence for stress triggering. We have applied this test to the November 24, 1987, Elmore Ranch/Superstition Hills earthquake sequence and find that those post-mainshock events that experienced stress increases of at least 0.01–0.03 MPa (0.1–0.3 bar) or that occurred from 1.4 to 2.8 years after the mainshocks are consistent with having been triggered by mainshock-generated static stress changes.

## 1. Introduction

The existence of aftershock sequences following large earthquakes shows that one earthquake can influence the rate of nearby seismicity, though the mechanisms responsible are not clearly understood; analogous effects may also occur over larger spatial and temporal scales. Possible triggers for such effects include dynamic strains generated by seismic waves [e.g., *Hill et al.*, 1993; *Anderson et al.*, 1994; *Gomberg and Bodin*, 1994], increased or decreased pore pressure [e.g., *Nur and Booker*, 1972; *Li et al.*, 1987; *Hudnut et al.*, 1989; *Noir et al.*, 1997], and changes in the regional static stress field [e.g., *Rybicki*, 1973; *Stein and Lisowski*, 1983; *King et al.*, 1994; *Harris*, 1998]. We discuss the last mechanism, static stress triggering, in this paper.

## 2. Static Stress Triggering

Coseismic static stress changes generated by large earthquakes alter the stress state in the nearby region and, if the induced stress changes are large enough, may

also affect seismicity. It is reasonable to expect that if the coseismic stress change increases the stress in an area, earthquakes might occur there sooner than they otherwise would have; conversely, if the stress decreases, subsequent events might be delayed. This effect would appear as an increased number or rate of subsequent smaller earthquakes (aftershocks and more regional seismicity) in places where the coseismic stress increment is positive, and fewer events or a lower seismicity rate in areas of stress decrease.

Most studies in this field use similar procedures for computing mainshock-induced stress changes. Given the slip distribution of the mainshock, the theory of elastic deformation from dislocations in a half-space [*Okada*, 1992] is used to compute coseismic stress increment tensors at specified locations. Next, these stress tensors are converted into the scalar Coulomb failure stress [e.g., *Jaeger and Cook*, 1979; *Scholz*, 1990], also known as the Coulomb failure function (CFF), on “target” faults with specified orientation and slip direction.

The change in CFF is commonly defined as

$$\Delta\text{CFF} = \Delta\sigma_s + \mu(\Delta\sigma_n + \Delta p), \quad (1)$$

where  $\Delta\sigma_s$  is the coseismic change in shear stress in the direction of fault slip,  $\Delta\sigma_n$  is the change in normal stress (with tension positive),  $\Delta p$  is the change in pore-fluid pressure, and  $\mu$  is a ‘‘coefficient of internal friction.’’

Equation (1) can be simplified by relating  $\Delta p$  to  $\Delta\sigma_n$  using Skempton’s coefficient  $B$ , which gives the change in pore-fluid pressure caused by a given coseismic stress change [Skempton, 1954; Rice and Cleary, 1976; Roeloffs, 1988]. Typically,  $B$  is contained implicitly in a new ‘‘effective coefficient of friction’’ defined as

$$\mu' = \mu(1 - B), \quad (2)$$

which reduces equation (1) to

$$\Delta\text{CFF} = \Delta\sigma_s + \mu'\Delta\sigma_n, \quad (3)$$

which is the commonly used form of the definition for  $\Delta\text{CFF}$ . We note that despite the wide usage of equation (3), it is important to keep in mind that this expression only holds under the assumption that  $\Delta\sigma_n$  and  $\Delta p$  are related in this simple manner.

One must know both the orientation (strike and dip) of and sense of slip (rake) on the ‘‘target’’ fault of interest in order to calculate  $\Delta\text{CFF}$ . Previous workers have taken three approaches to determine these parameters: (1) use of a priori information on fault location, orientation, and slip direction, usually from geologic data; (2) use of the nodal plane orientation and slip information from the focal mechanism for a potentially triggered earthquake; and (3) making the assumption that faults of all orientations exist everywhere in the region and that earthquakes are most likely to occur on faults whose orientations and slip directions are ‘‘optimal’’ for failure. The third method requires knowledge of the background stress field, while the other two do not.

The first method is appropriate for studying the influence of induced stress changes on the occurrence of future mainshocks along other faults [e.g., Stein *et al.*, 1997], and we will not discuss it further. Several authors have used the two other techniques to explore static stress triggering of aftershocks and regional seismicity. These workers have found that  $\Delta\text{CFF}$  correlates well in a qualitative sense with the observed distribution of earthquakes following the 1979 Homestead Valley, 1984 Morgan Hill, 1989 Loma Prieta, 1992 Landers, and 1994 Northridge earthquakes in California [Stein and Lisowski, 1983; Oppenheimer *et al.*, 1988; Harris and Simpson, 1992; Reasenberg and Simpson, 1992; Stein *et al.*, 1992; King *et al.*, 1994; Stein *et al.*, 1994; Reasenberg and Simpson, 1997; Hardebeck *et al.*, 1998], the 1954 Fairview Peak/Dixie Valley events in Nevada [Hodgkinson *et al.*, 1996; Caskey and Wesnousky, 1997],

and the 1995 Kobe shock in Japan [Toda *et al.*, 1998], among others. These studies have shown that static stress triggering is consistent with the pattern of most of the aftershocks of these large earthquakes (typically 70–80%), that  $\Delta\text{CFF}$  levels of 0.01–0.02 MPa (0.1–0.2 bar) are necessary for significant triggering, and that coseismic static stress changes can significantly trigger seismicity for 6 months to more than 4 years following the mainshock. We refer the interested reader to Harris [1998], who gives a detailed review of static stress triggering.

### 3. Quantitative Tests for Static Stress Triggering

The correlations noted above certainly suggest that static stress triggering may play a role in some aftershock sequences, but it is not known if such triggering is generally present and how important an effect it may be. Some workers have developed quantitative methods for determining the importance of stress triggering during aftershock sequences and have reached different conclusions. Here, we give a short review of some of those conclusions.

Beroza and Zoback [1993] and Kilb *et al.* [1997] found that static stress triggering following the Loma Prieta mainshock could not be reliably used to explain the diversity of focal mechanisms exhibited by Loma Prieta aftershocks. However, seismicity rate and Loma Prieta-generated  $\Delta\text{CFF}$  patterns have been found to correlate well on more regional scales in central California [Reasenberg and Simpson, 1992, 1997]. Hardebeck *et al.* [1998] asked whether the percentage of aftershocks consistent with triggering caused by the Landers and Northridge earthquakes was higher than might be expected from random chance and showed that for the Landers aftershocks the percentage was significantly higher, while for the Northridge events it was not. Gross and Kisslinger [1994] concluded that differences in the distributions of  $\Delta\text{CFF}$  values for regional seismicity preceding and following moderate earthquakes in the central Aleutian Islands were significant and consistent with triggering by those events. Toda *et al.* [1998] showed that regional seismicity rate changes following the Kobe earthquake could be explained by the coseismic stress changes generated by the Kobe mainshock. Table 1 summarizes of these tests.

Clearly, these methods have returned mixed results. For the Loma Prieta and Northridge aftershocks, static stress triggering appears not to be a significant influence. On the other hand, static stress triggering seems to have played an important role during the Landers and Kobe aftershock sequences and more generally in the Aleutian arc and regionally in central California following the Loma Prieta mainshock. We note here

that it would be interesting to apply each test to a uniform set of earthquakes and then compare the results; so far, this has not been done, and so we cannot decide if the differences are due to the earthquakes or the tests. For now, we suggest that while the studies cited in section 2 are tantalizing, static stress triggering has not yet been conclusively proven an important effect. Additional work is needed, and in the remainder of this paper we discuss a test for static stress triggering that we have developed and applied to yet another aftershock sequence, that following the November 24, 1987, Elmore Ranch/Superstition Hills earthquakes.

#### 4. Stress Distribution Test

In this section we detail our method for testing the static stress triggering hypothesis. We use the Kolmogorov-Smirnov (KS) test to compare the statistical distribution of  $\Delta\text{CFF}$  values computed for a set of post-mainshock events to the distribution of  $\Delta\text{CFF}$  values computed identically for a set of pre-mainshock events; if we can reject the hypothesis that these distributions are the same, our data are consistent with static stress triggering. We call this technique the stress distribution (SD) test. Section 5 gives three synthetic examples to help illustrate our method, and the appendix discusses the KS test for readers who may not be familiar with it.

We begin by selecting a catalog of earthquakes which occurred between July 1983 and December 1997 within a 100-by-100 km box surrounding the epicenters of the Elmore Ranch/Superstition Hills (ERSH) mainshocks; these are typical temporal and spatial scales one might choose in extracting data sets for use with our technique. Our catalog contains both events before the mainshock (which we call preshocks) and events which follow the mainshock (which we call postshocks), selected using identical criteria in both time periods. We choose the names preshocks and postshocks to distinguish these events from foreshocks and aftershocks, since the preshocks and postshocks occur over much larger areas and longer times than the terms foreshocks and aftershocks traditionally denote.

The ERSH event catalog contains both location and phase pick information and from these, we compute first-motion fault plane solutions (FPS) using the FPFIT computer program of *Reasenber and Oppenheimer* [1985]. From the initial set of focal mechanisms we reject FPS with strike, dip, or rake uncertainties  $> 30^\circ$  and station distribution ratios (STDR)  $< 0.4$  [see *Reasenber and Oppenheimer*, 1985]. FPFIT often gives multiple FPS for a given event; we keep only the one with the highest STDR and lowest misfit between observed and predicted first-motion polarities.

Once we have culled the best events and FPS from

our initial set, we use the dislocation code DIS3D [*Erickson*, 1986] and an assumed slip model for the mainshock to compute the coseismic stress increment tensor at the hypocenter of every event in our data set. We combine these stress increment tensors with the FPS for each event and calculate the observed Coulomb stress change ( $\Delta\text{CFF}$ , given by equation (3)) on each of the two FPS nodal planes, assuming a fixed value for  $\mu'$ . In order to reduce the effect of uncertainties in the mainshock slip distribution on our  $\Delta\text{CFF}$  estimates we remove from our set any event nearer than a few kilometers to the mainshock fault plane. In the specific case of the ERSH events we assume  $\mu' = 0.4$  and remove events closer than 2.5 km to either mainshock fault plane.

We also find the maximum and minimum  $\Delta\text{CFF}$  possible (given our choice of  $\mu'$ ) for an arbitrarily oriented fault plane with arbitrary rake at each hypocentral location and use these extremal stresses to normalize the observed values. We normalize by dividing positive  $\Delta\text{CFF}$  values by the maximum possible  $\Delta\text{CFF}$  (which is always positive) and negative  $\Delta\text{CFF}$  values by the minimum possible  $\Delta\text{CFF}$  (which is always negative) and preserve the original sign of  $\Delta\text{CFF}$  so that positive  $\Delta\text{CFF}$  values map into the range from 0 to +1 and negative values from -1 to 0. We call the results the normalized  $\Delta\text{CFF}$  (NCFF) values. Figure 1 shows a flowchart of the preprocessing steps.

Our main reason for normalizing the  $\Delta\text{CFF}$  values is to treat all potentially triggered earthquakes equally; every event should have equal weight, in our opinion, and the following example should illustrate why. The magnitude of the stress increment due to a mainshock falls off as a function of distance from the main rupture plane or planes. This means that the possible range of  $\Delta\text{CFF}$  values for nearby postshocks is considerably larger than the range for distant postshocks. It is possible, therefore, for  $\Delta\text{CFF}$  values for non-optimally oriented nearby earthquakes to be numerically larger than  $\Delta\text{CFF}$  for very optimally oriented distant events. Clearly, in this case, the distant event should be considered more consistent with the stress triggering hypothesis than the nearby event, but without normalization this will not be the case. We feel this effect is sufficiently important that it should be considered, in one form or another, in all tests of stress triggering which make use of the Coulomb failure stress and event fault plane solutions.

One could argue that it is artificial to compute  $\Delta\text{CFF}$  and NCFF values for the preshocks, as they occurred before the mainshock. However, the postshocks are not just the result of the coseismic static stress increment from the mainshock but also will contain events which would have happened regardless of the mainshock's occurrence, simply due to background tectonic stresses. Since we wish to determine whether or not the coseis-

**Table 1.** Selected Tests for Static Stress Triggering

Reference	Method Summary	Data and Parameters Used	Triggering Significant?
<i>Beroza and Zoback</i> [1993]	compared mainshock-induced stress tensors computed at aftershock hypocenters to observed aftershock moment tensors; aftershocks with positive stress change and consistent tensors were considered consistent with triggering	Loma Prieta aftershock hypocenters and moment tensors	no
<i>Gross and Kisslinger</i> [1994]	computed $\Delta$ CFF induced by “target” events on optimal planes located at hypocenters of nearby regional seismicity*; used $t$ statistics to compare the distribution of $\Delta$ CFF values for events before and after each “target” event and tested significance of $\Delta$ CFF distribution changes using bootstrap method	central Aleutian Islands event hypocenters and times, 1974–1986	yes
<i>Kilb et al.</i> [1997]	estimated optimal focal mechanisms from maximum mainshock-induced $\Delta$ CFF at aftershock hypocenters*; compared estimated to observed mechanisms for same events and used bootstrap technique to estimate significance of positive correlations between corresponding mechanisms	Loma Prieta aftershock hypocenters and focal mechanisms	no
<i>Reasenber and Simpson</i> [1992, 1997]	computed $\Delta$ CFF on 200 fault planes representing large regional faults and correlated $\Delta$ CFF with observed seismicity rate change; used fourfold $\chi^2$ test to estimate significance of observed positive correlation	pre- and post-Loma Prieta epicenters and times, a priori fault planes	yes
<i>Hardebeck et al.</i> [1998]	computed $\Delta$ CFF on focal mechanism nodal planes at aftershock hypocenters and computed percentage of aftershocks with positive $\Delta$ CFF and did the same for synthetic aftershock sequences based on the real aftershocks; if observed percentage was significantly higher than synthetic percentage, sequence was considered consistent with triggering	Northridge (N) and Landers (L) aftershock hypocenters and focal mechanisms	N, no L, yes
<i>Toda et al.</i> [1998]	computed $\Delta$ CFF on optimal fault planes at grid points in a volume around Kobe mainshock*; correlated $\Delta$ CFF with observed seismicity rate change and used fourfold $\chi^2$ test to estimate significance of observed positive correlation	pre- and post-Kobe epicenters and times, optimal fault planes*	yes

\*“Optimal” fault planes are those planes whose orientation and slip directions combine to give the maximum possible  $\Delta$ CFF at a given location using a given mainshock slip distribution model and a given value of  $\mu'$ . One must know both the mainshock-induced  $\Delta$ CFF values and the background stress field in order to compute the optimal fault planes or optimal focal mechanisms.

## Initial events and fault plane solutions (FPS)

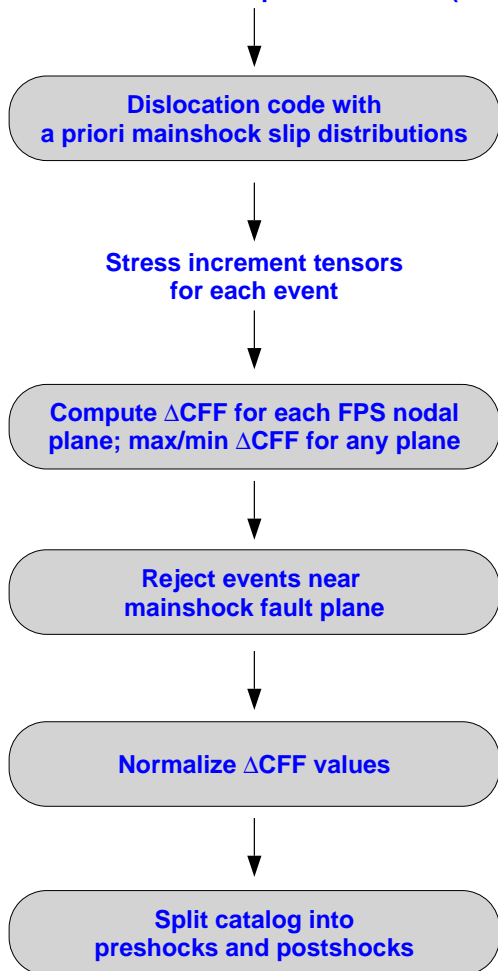


**Figure 1.** Preprocessing steps for the SD test. Boxes represent steps at which some manipulation of the data occurs. See text for details.

mic static stress changes drive additional seismicity, we need to have a representative set of background events which could not have been affected by the mainshock; the preshocks provide just such a set. We therefore use the NCFE values from the preshocks for comparison with the NCFE values from the postshocks.

There are two additional complications in applying the SD test. Owing to the fundamental ambiguity in choosing which of the two possible FPS nodal planes best represents the actual rupture plane, we cannot decide which of a given event’s two NCFE values to use without additional a priori information (note that this ambiguity does not exist when  $\mu' = 0$ ). Also, since the SD test is based on comparing a given set of postshocks to a given set of preshocks, we face the issue of how a particular choice of events affects the outcome. Both of these problems must be addressed, and we choose to do so using a bootstrap resampling technique [Efron,

1982; Efron and Tibshirani, 1986] in which we generate synthetic data sets using our observed preshock and postshock catalogs. To do so for either the preshocks or postshocks, we make a random selection of events, and for each event we randomly select one of the two possible NCFE values. (The number of events in each bootstrap resampling depends on the particular application but in all cases is the same as in the observed data set.)

We now compare the distribution of a set of postshock bootstrap NCFE values to that of a bootstrap resampling of preshocks and do so using the cumulative distribution functions (CDFs) for each set of NCFE values. We compute empirical CDFs for the preshock and postshock bootstrap NCFE estimates using equation (A1), and then compare these CDFs using the Kolmogorov-Smirnov (KS) test as in the appendix (equations (A2)–(A6)). The KS test gives the confidence with which we can reject the null hypothesis that the preshock and postshock bootstrap NCFE values are drawn from the same distribution; we call the KS rejection level  $P_{KS}$  (see equation (A3)). We repeat this process of choosing a bootstrap sample of the preshock and postshock NCFE values, computing the CDF for each sample, and comparing the CDFs with the KS test 10,000 times and, in so doing, develop an estimate of the effects of our particular event selection and of possibly mischoosing the “correct” FPS nodal plane. Figure 2 shows these steps in graphical form.

Through the above process, we assemble a set of 10,000  $P_{KS}$  values which are estimates of the rejection level for the null hypothesis that the preshock and postshock CDFs are the same; we call these the  $P_{KS}^{obs}$ . We next examine the CDF for the  $P_{KS}^{obs}$  values themselves. This may appear unusual, as the distribution of a single probability estimate is a meaningless concept. However, each  $P_{KS}^{obs}$  estimate is derived from applying the same test to a different synthetic data set and thus can be treated as a separate member of a population; the distribution of this population can be described using a CDF.

The final step in the SD test is to use the KS test to compare the CDF of the  $P_{KS}^{obs}$  values with the CDF of some reference set of KS rejection levels, the  $P_{KS}^{ref}$ , which will vary depending on the specific circumstances, but which are generally derived by comparing two or more subsets of the preshocks to one another. For example, the most fundamental question in any study looking for static stress triggering is whether or not the results of the given test for the preshock/postshock comparison are different from what one would have found in the absence of the mainshock. As mentioned previously, comparing CDFs of different subsets of preshocks to one another can provide an estimate of  $P_{KS}^{ref}$  because these events cannot have been influenced by the mainshock.

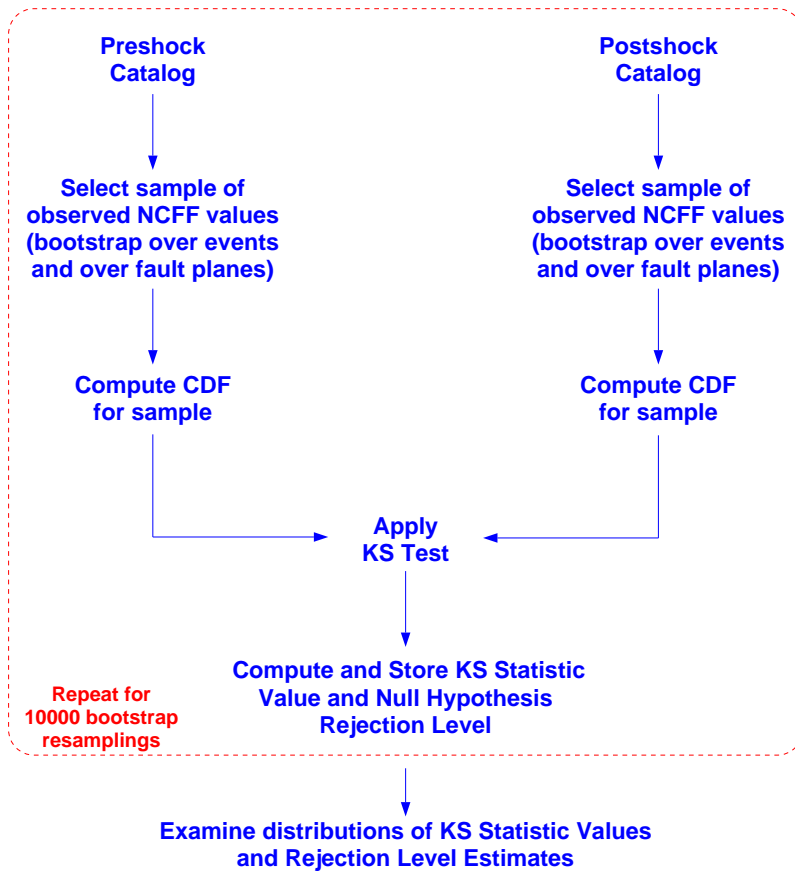


**Figure 2.** Schematic diagram of the SD test. The steps contained within the dashed box are the bootstrap resampling and application of the KS test, which are both repeated 10,000 times. After the data have been resampled 10,000 times and the KS test has been performed on each set, the results are examined as described in the text.

We now state our definition of “significant static stress triggering,” which has three parts:

1. The envelope of CDFs for the bootstrap resamplings used to calculate  $P_{\text{KS}}^{\text{obs}}$  is shifted toward higher NCFV as compared to the CDF envelope for the  $P_{\text{KS}}^{\text{ref}}$  bootstrap resamplings.

2. The KS-test rejection level for the hypothesis that  $P_{\text{KS}}^{\text{obs}}$  and  $P_{\text{KS}}^{\text{ref}}$  are drawn on the same distribution is greater than 95%.

3. The  $P_{\text{KS}}^{\text{obs}}$  CDF is skewed toward higher rejection levels than is the  $P_{\text{KS}}^{\text{ref}}$  CDF.

All of these must be present for us to declare a data set consistent with static stress triggering. In section 5, we give three synthetic examples to illustrate the behavior of the SD test under a variety of limiting conditions and in section 6 we apply the SD test to the Elmore Ranch/Superstition Hills earthquakes.

## 5. Synthetic Examples

In this section we present three synthetic examples designed to show the behavior of the SD test under

various conditions: (1) the underlying statistical distribution of the first data set,  $P_1$ , is the same as that of the second,  $P_2$  (i.e.,  $P_1 = P_2$ ), and we have one sample of data from which we draw bootstrap resamples; (2)  $P_1 = P_2$  and we have two independent samples of data drawn on this distribution; and (3)  $P_1 \neq P_2$  and we have one data set drawn on each distribution. We have constructed these examples to encompass the full range of behaviors which might be expected, from a situation in which we know the null hypothesis to be correct (example 1) to one in which we know we can reject it (example 3). Note that in each of these examples the null hypothesis is always that the data samples are drawn on the same underlying statistical distribution.

In the first example, both the preshocks and postshocks are drawn on the same underlying Gaussian distribution (shown in Figure 3a). We begin by drawing one random sample of 500 pairs of data points from this distribution; each pair of data points represents the two NCFV values from a single event (two NCFV values because of the focal mechanism ambiguity), and we select 500 such pairs to approximately match the

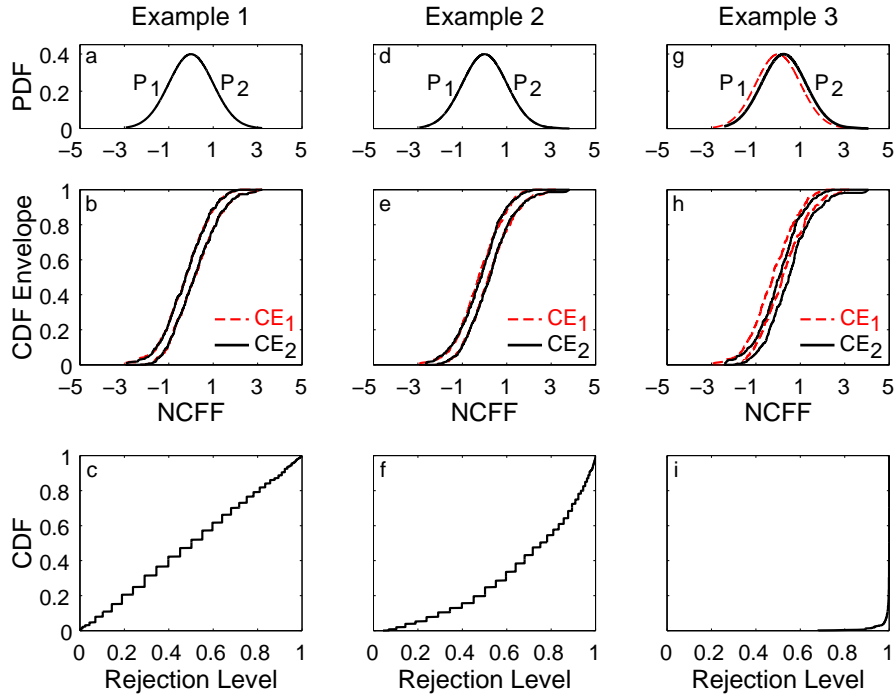


**Figure 3.** Synthetic examples for the SD test. (a) Underlying distributions ( $P_1$  and  $P_2$ ) for the synthetic preshocks and postshocks, respectively. Note that in this case,  $P_1 = P_2$ . (b) Complete envelope (CE) for all 10,000 CDFs generated by bootstrap resampling of the preshocks (paired dashed lines;  $CE_1$ ) and postshocks (paired solid lines;  $CE_2$ ), which were drawn from a single realization of  $P_1$ . Note that  $CE_2$  overlies  $CE_1$  exactly and so  $CE_1$  is not visible. (c) CDF for the KS test rejection levels from each of the bootstrap resamplings. Note that KS rejection levels are distributed uniformly. (d)  $P_1$  and  $P_2$  for the second example. In this case, as in the first example,  $P_1 = P_2$ , but we have two realizations of data drawn on that distribution. (e) As in Figure 3b, except that the preshock and postshock data are drawn independently from the same distribution as described above. (f) CDF for KS test rejection levels. Note that KS rejection levels are no longer distributed uniformly (see text). (g)  $P_1$  and  $P_2$  for the third example; in this case,  $P_1 \neq P_2$ . (h) As in Figure 3b, except that the preshock and postshock data are drawn independently from two different distributions, as described above. (i) CDF for KS test rejection levels.

number of events in the data presented later. From this 500-pair random sample, we select 500-point bootstrap resamplings for both preshocks and postshocks by first randomly selecting pairs and then randomly choosing between the members of a given pair, exactly as described in section 4. We then compute CDFs for these bootstrap resamplings and compare these CDFs as described in section 4; Figure 3b shows the complete envelopes of the two sets of bootstrap CDFs (rather than showing all 10,000 CDFs themselves), which overlie one another in this case. Figure 3c shows the CDF of the KS test rejection levels (the CDF of the  $P_{KS}$  values). In this case, the  $P_{KS}$  estimates are distributed uniformly over the range 0 to 1, as might be expected.

In the second example, both preshocks and postshocks are again drawn on the same underlying Gaussian distribution, shown in Figure 3d, but we now generate two random samples of 500 pairs of data points each and process these “events” through the SD test as with the first example. We again show the complete

envelope of the bootstrap CDFs (rather than all 10,000 bootstrap CDFs themselves) in Figure 3e, and Figure 3f shows the CDF of the  $P_{KS}$  estimates. Interestingly, the  $P_{KS}$  values are no longer uniformly distributed, even though both data sets are drawn on the same distribution. This is the effect of drawing two sets of only 500 events each from the analytical distribution; had we drawn two much larger samples, this example would become the same as the first and the  $P_{KS}$  would tend to a uniform distribution. In other words, 500 samples are statistically insufficient to characterize the analytic distribution in this case.

In the third example the underlying distributions for the two data sets are different by a small amount (Figure 3g). We again generate two random data sets of 500 pairs of data points each, with one set of events based on  $P_1$  and the other on  $P_2$ , select 500-point bootstrap resamplings from them, and compare the CDFs for the resamplings. Clearly, the CDF envelope for the  $P_2$  resamplings is shifted toward higher NCCF values than

is the  $P_1$  CDF envelope (Figure 3h), and the CDF for  $P_{KS}$  is significantly more peaked toward high rejection level than when the two data sets are drawn on identical distributions (Figure 3i). The behavior displayed in Figures 3h and 3i is similar to that which would be expected under the SD test if significant static stress triggering were present.

## 6. Results and Discussion

We now use the SD test to search for significant static stress triggering during one southern California earthquake sequence: the November 24, 1987, Elmore Ranch/Superstition Hills (ERSH) events, southwest of the Salton Sea in the Imperial Valley (Figure 4). The Elmore Ranch shock ( $M$  6.2, 0154 UT) ruptured a SW-NE trending strike-slip fault; inversions of geodetic data are consistent with 30 cm of left-lateral slip along a vertical fault striking  $N40^\circ E$ . The Superstition Hills shock ( $M$  6.6, 1315 UT) broke a NW-SE trending strike-slip fault; inversions of geodetic data are consistent with about 1.3 m of right-lateral slip along a vertical fault striking  $N50^\circ W$  [Larsen *et al.*, 1992]. These two faults form a conjugate pair, and it seems likely that the Elmore Ranch event (ER) triggered the Superstition Hills event (SH) by lowering the normal stress along the Superstition Hills fault by as much as 0.5–1 MPa (5–10 bars) [Hudnut *et al.*, 1989; Larsen *et al.*, 1992]. This sequence is discussed extensively in a special issue of the *Bulletin of the Seismological Society of America* [Hanks and Allen, 1989].

Our ERSH data set consists of events recorded by the Southern California Seismic Network (SCSN) in the Imperial Valley and surrounding regions from July 1983 (4.2 years prior to the ER event and the earliest data with phase pick information available in the catalog) through December 1997 (10 years after the SH event). We initially select 4432  $M \geq 2.0$  events with horizontal location errors  $\leq 2.0$  km and vertical location errors  $\leq 3.0$  km and process them as shown in Figure 1 to arrive at the final data set of 1275 earthquakes, 387 of which are preshocks and 888 of which are postshocks.

We choose model 2b from Larsen *et al.* [1992] as the slip distribution for the ER and SH mainshocks. This model is derived from repeated Global Positioning System (GPS) geodetic observations spanning the time of the ERSH events at 30 sites in and near the Imperial Valley and has two fault planes, one representing the ER event and the other the SH event. Both the ER and SH fault planes are 25 km long, extending vertically from the surface to 10 km depth. Each fault is divided into 50 rectangular subfaults, with the ER model slip plane striking  $N40^\circ E$  and the SH plane striking  $N50^\circ W$ . We note here that our choice of slip model no doubt influences our results and that other slip models could result

in somewhat different conclusions than we show below (as discussed by, for example, Reasenber and Simpson [1992, 1997]).

### 6.1. Overall Results

We first apply the SD test to the entire ERSH data set to determine whether or not there is evidence of significant static stress triggering for the complete set of events. We split the ERSH data into preshocks and postshocks and process both sets using the SD test as in the third synthetic example given in section 5, arriving at a set of  $P_{KS}^{obs}$  estimates which we then need to compare to a set of  $P_{KS}^{ref}$  estimates.

In this case, we generate the  $P_{KS}^{ref}$  estimates by comparing subsets of the preshocks to one another. In doing so, however, we face the complication that the  $P_{KS}^{ref}$  estimates computed by comparing a given pair of preshock subsets to each other can vary significantly from the  $P_{KS}^{ref}$  estimates calculated by comparing two other subsets to one another. Such differences reflect temporal variability in the preshocks caused by the statistical non-stationarity in the occurrence of earthquakes (over short time periods); clearly, any triggering effect would need to stand out above this background variability.

We choose to address this issue by splitting the preshocks into three equal 1.4-year bins and performing all unique bin-to-bin comparisons using the SD test, which results in a set of three  $P_{KS}^{ref}$  CDF estimates. Figure 5 shows maps of the events in each time bin. Obviously, we would like to have as many subsets of the preshocks as possible (many bins), but we are limited in the number of bins by the need to have sufficient events in each bin (approximately 100) to make meaningful estimates of  $P_{KS}^{ref}$ . Thus while our choice of three bins may seem arbitrary, it is in fact a good compromise between these two competing needs. We have experimented with various changes to the bin boundaries and the number of time bins and have tried binning by equal numbers of events, rather than equal lengths of time, and have found that the patterns we see in the  $P_{KS}^{ref}$  and  $P_{KS}^{obs}$  estimates remain similar to those discussed below.

Figure 6 shows the four resulting distributions, with the  $P_{KS}^{obs}$  CDF shown as the thick line and the  $P_{KS}^{ref}$  CDF estimates shown as thin lines. Clearly, the  $P_{KS}^{obs}$  CDF estimate lies within the range of the three  $P_{KS}^{ref}$  CDF estimates. We conclude from the results shown in Figure 6 that our data set taken as a whole is inconsistent with the static stress triggering hypothesis. That is, the amount of variability in  $P_{KS}^{ref}$  simply due to the “normal” fluctuations from the non-stationarity of the preshocks is larger than the potential stress triggering signal contained in the post-mainshock interval for the ERSH data set taken as a whole.

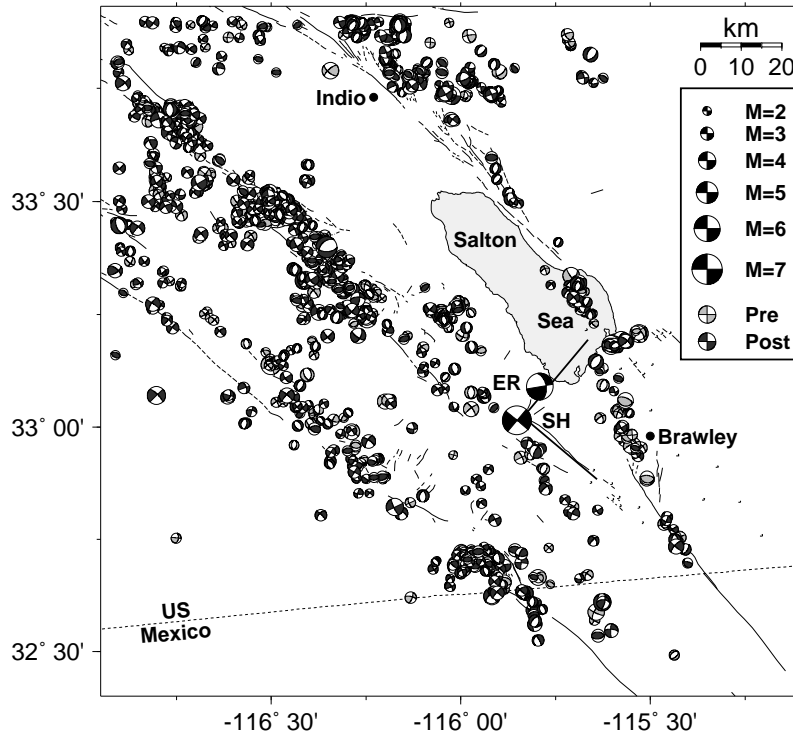


**Figure 4.** Seismicity and faults in and near the Imperial Valley. Events are shown as focal mechanisms, with pre-ERSH (July 13, 1983 to November 23, 1987) earthquakes shaded and post-ERSH (November 24, 1987 to December 31, 1997) events solid. Elmore Ranch and Superstition Hills mainshock focal mechanisms are labeled ER and SH, respectively. Heavy solid lines denote the *Larsen et al.* [1992] dislocation model slip planes. Salton Sea, Indio, Brawley, and the United States/Mexico border are shown for reference. Focal mechanisms scale with magnitude as shown in the legend at right.

## 6.2. Duration of Significant Triggering

While the data taken together are inconsistent with static stress triggering, there may be some subset of the ERSH postshock data set that is consistent with triggering and which may be overwhelmed by the rest of the data when they are examined simultaneously. One obvious way to search for such subsets is to divide the postshocks into shorter time windows.

We subdivide the postshocks into seven equal bins of 1.4 years each (see Figure 7) and compare the events in each bin to all of the preshocks using the SD test; in so doing, we compute a  $P_{KS}^{obs}$  CDF estimate for each of the seven bins. We compare each of these seven  $P_{KS}^{obs}$  CDFs to the same three  $P_{KS}^{ref}$  CDFs used above, which were computed by comparing bins of preshocks to one another. Figure 8 shows the results, with the  $P_{KS}^{obs}$  CDFs shown as thick lines and the  $P_{KS}^{ref}$  CDFs shown as thin lines. Note that all but one of the  $P_{KS}^{obs}$  CDFs are either within the range of the  $P_{KS}^{ref}$  CDFs or are less consistent with triggering (i.e., closer to a uniform distribution).

The second  $P_{KS}^{obs}$  CDF estimate lies outside the range of the  $P_{KS}^{ref}$  CDFs and is shifted toward higher rejection levels (cf. dashed line in Figure 8). We compare this  $P_{KS}^{obs}$  CDF to the most “triggering-like” (i.e., shifted farthest to the right)  $P_{KS}^{ref}$  CDF using the KS test and find that we can reject the hypothesis that these CDFs are the same with much greater than 99% confidence. Though not shown, it is also the case that the envelope of individual bootstrap CDFs for this single preshock/postshock comparison is shifted toward higher NCFF values than is the envelope for the preshock/preshock comparison. Given these three observations, we conclude that there was significant static stress triggering for events during this second time bin (1.4–2.8 years after the mainshock) but not in the first or third through seventh bins. However, note that we only have three estimates of the  $P_{KS}^{ref}$  curves, and it is possible that with a longer span of preshock data, and thus more than three time bins for the comparison, other preshock/preshock comparisons could result in a

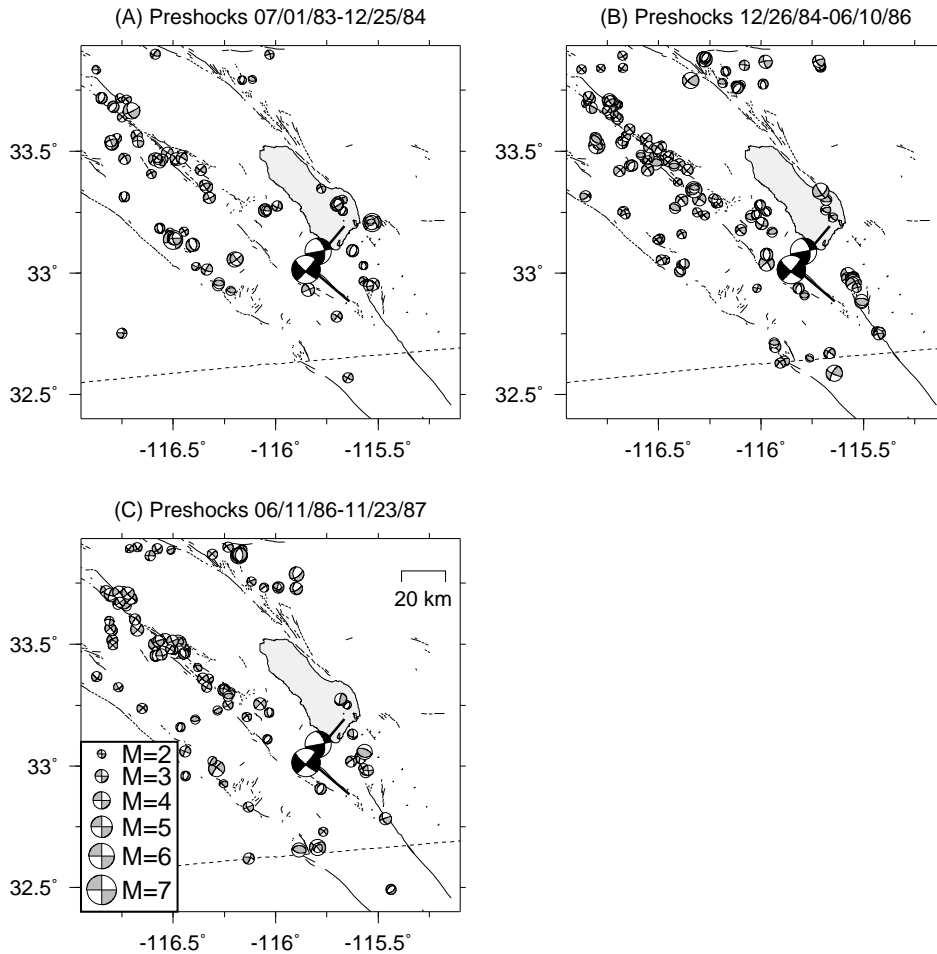


**Figure 5.** ERSH preshocks, divided into three equal 1.4-year time bins. Events are shown as focal mechanisms, which scale with magnitude as shown in the legend in Figure 5c. Elmore Ranch and Superstition Hills mainshocks are shown as large solid focal mechanisms. Heavy solid lines denote the *Larsen et al.* [1992] dislocation model slip planes. Salton Sea and the United States/Mexico border are shown for reference. (a) Events in first time bin. (b) Second time bin. (c) Third time bin.

$P_{KS}^{\text{ref}}$  shifted farther to the right, which would reduce our confidence in this conclusion. We have no way to evaluate this possibility with the current data set.

If the above conclusion is correct, it is an unexpected result, because if our model of static stress triggering is correct, we would expect the triggering effect to be strongest immediately following the mainshock and to taper off with time. One possible explanation is a localized swarm of events with favorable focal mechanisms which all happen to occur during this time bin, but we have examined the spatial and temporal distributions of the seismicity in this time bin and find no evidence for such swarming (compare Figure 7b with the other maps in Figure 7). Another possibility is that there is some physical mechanism which delays the onset of triggering, such as pore-fluid propagation [e.g., *Nur and Booker, 1972; Noir et al., 1997*], but the time and dis-

tance ranges involved in this data set make such an explanation seem unlikely. One could also speculate that these events were on the verge of failure at the time of the ERSH mainshocks and were retarded by the coseismic stress increment by about 1.4 years' worth of background stress accumulation, but this seems somewhat implausible. We are left with the conclusion that significant triggering occurred during the time period from 1.4 to 2.8 years following the ERSH mainshocks but not earlier or later during the postshock sequence; we currently have no adequate explanation for this temporal behavior.

### 6.3. Stress Threshold for Triggering

We next examine the possibility that there is a threshold of induced stress above which static stress triggering is a significant effect. We subdivide the

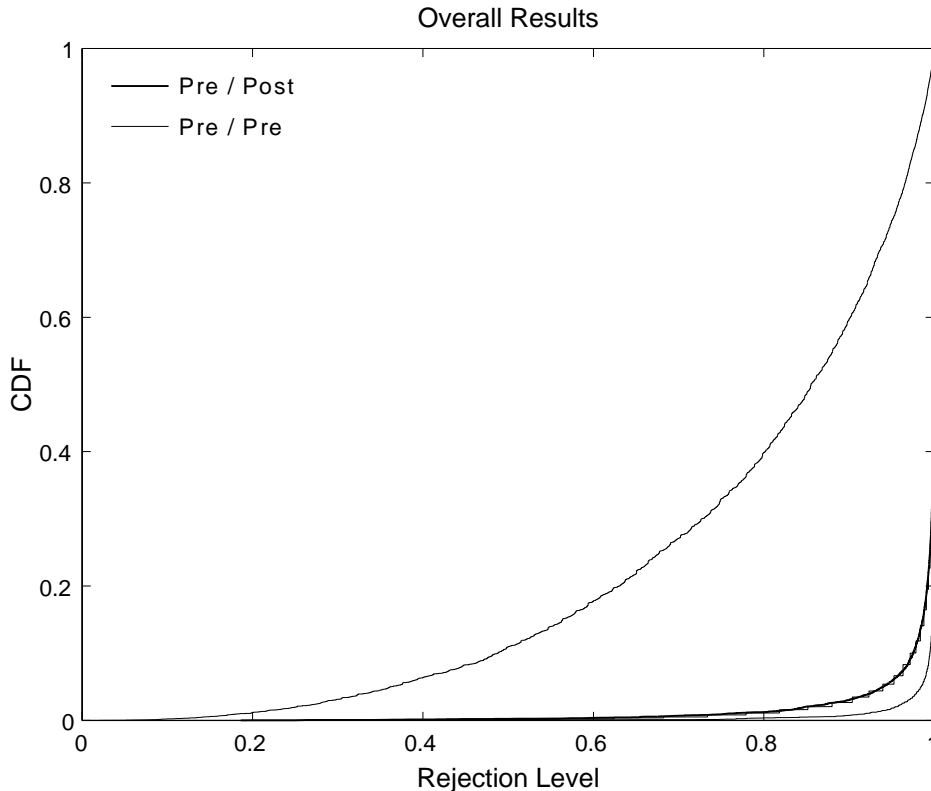


**Figure 6.** Results of applying the SD test to all ERSB events. Thick line is the CDF of  $P_{KS}^{obs}$  values computed by comparing all postshocks to all preshocks using the SD test. Thin lines are estimates of the  $P_{KS}^{ref}$  CDF generated by dividing the preshocks into three 1.4-year bins and making all unique bin-to-bin comparisons. Note that the  $P_{KS}^{obs}$  CDF lies within the range of  $P_{KS}^{ref}$  CDF estimates, which is inconsistent with significant static stress triggering.

preshocks and postshocks into three non-overlapping stress magnitude bins (0–0.01 MPa, 0.01–0.03 MPa, and 0.03 MPa or greater; 0–0.1, 0.1–0.3, and 0.3 bar or larger) and apply the SD test to the events in each bin independently, comparing the preshocks and postshocks and building up a set of  $P_{KS}^{obs}$  estimates. We then randomly divide the preshocks into two halves (a “random half division”), bin each half with the stress bins listed above, and apply the SD test to these baseline sets of events, resulting in a single set of 10,000  $P_{KS}^{ref}$  estimates for each stress bin. We are limited to splitting the preshocks in half by the need to have at least 100 events in each subset; splitting into more bins gives too few events for reliable  $P_{KS}^{ref}$  estimates. We have also attempted to check the possibility that we have made a particularly poor random half division of the preshocks, by generating several other such random half divisions and applying the above procedure. We have found no important changes to the results shown in Figure 9 (where the thick line in each panel represents the  $P_{KS}^{obs}$  CDF and the thin line represents the  $P_{KS}^{ref}$  CDF).

It is clear from Figure 9 that we observe no significant static stress triggering for stress magnitudes below 0.01

MPa (0.1 bar). However, the  $P_{KS}^{obs}$  and  $P_{KS}^{ref}$  CDF estimates for the 0.01–0.03 and 0.03 MPa and higher stress bins are significantly different at greater than the 99% level, the  $P_{KS}^{obs}$  CDF is shifted toward higher rejection levels than is the  $P_{KS}^{ref}$  CDF, and, though not shown, the bootstrap CDF envelope for the preshock/postshock comparison is shifted toward higher NCFV values than is the preshock/preshock bootstrap CDF envelope. By our definition, therefore, events within these stress bins are consistent with triggering. We have experimented with other stress bin limits and find that the pattern we see here is robust. We conclude that the minimum applied stress threshold for significant triggering during the ERSB sequence is about 0.01–0.03 MPa (0.1–0.3 bar), which is consistent with the results of earlier studies on different earthquake sequences.

## 7. General Issues for Tests of Static Stress Triggering

Some of the issues we face in using the SD test to search for the existence of static stress triggering are problems which any other test must also resolve, and thus warrant further emphasis. The first such issue

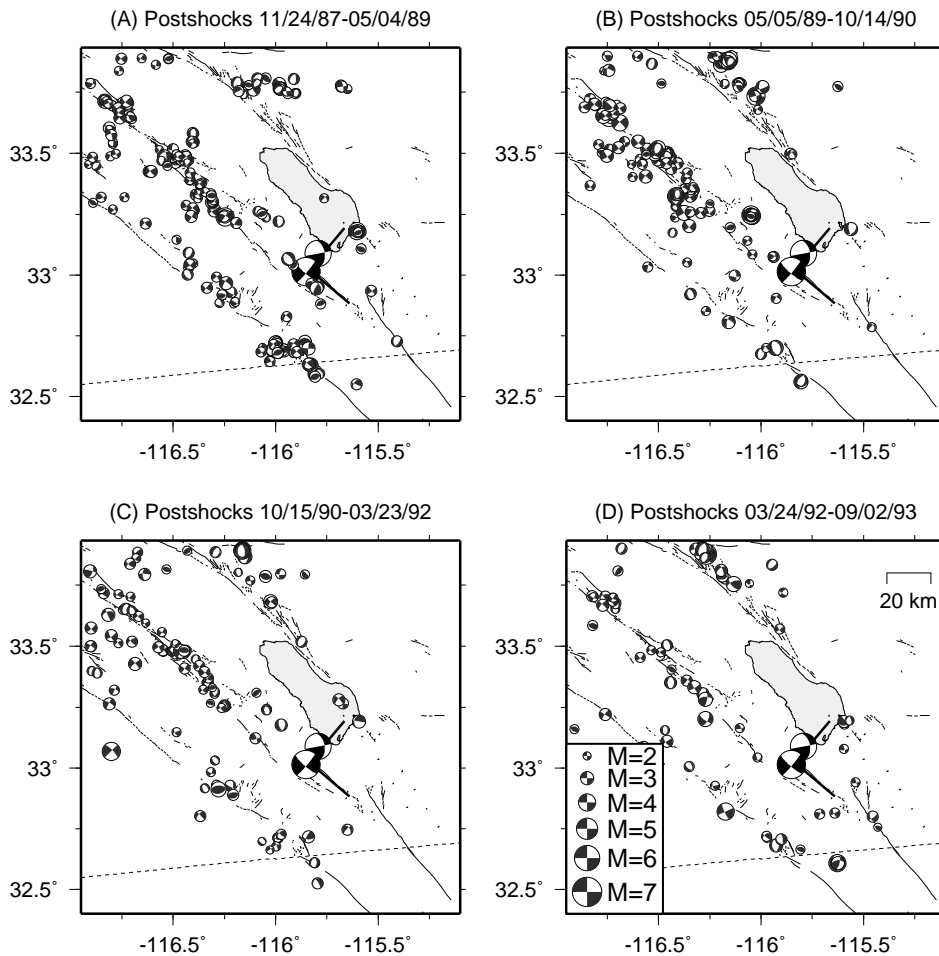


**Figure 7.** ERSH postshocks, divided into seven equal 1.4-year time bins. Events are shown as focal mechanisms, which scale with magnitude as shown in the legend in Figure 7d. Elmore Ranch and Superstition Hills mainshocks are shown as large solid focal mechanisms. Heavy solid lines denote the *Larsen et al.* [1992] dislocation model slip planes. Salton Sea and the United States/Mexico border are shown for reference. (a) Events in the first time bin. (b) Second time bin. (c) Third time bin. (d) Fourth time bin. (e) Fifth time bin. (f) Sixth time bin. (g) Seventh time bin.

arises for tests in which stress changes are computed using event focal mechanism information. For every event focal mechanism, there are two nodal planes, each of which could be the rupture plane; this leads to two distinct values of coseismic Coulomb stress change (unless  $\mu' = 0$ ). In the usual absence of other information, it is not possible to choose which of the two nodal planes best approximates the true rupture plane and thus which stress change value is most correct. Thus tests for triggering either must not use focal mechanism information or must be designed to handle this fundamental ambiguity.

Any test for static stress triggering will consist of comparing a postshock set of earthquakes to some reference data set. Clearly, we require as large a number of events as possible, over the longest period of time

possible, in order to make reliable comparisons between these two data sets; exactly what constitutes a “large” number of events and a “long” period of time will depend on the details of a given situation. However, what does not depend on the situation, and is perhaps not as clear, is that if we wish to draw meaningful conclusions from the data set comparisons, we must also have a set of reference events which adequately represents the true regional background seismicity. This is because static stress triggering is a secondary effect superimposed on the background tectonic forces which primarily drive the seismicity in a given region. Any postshock data set will contain events whose occurrence is unrelated to the mainshock, and without knowing this background rate correctly, we cannot hope to meaningfully test for the existence of additional events driven by static stress

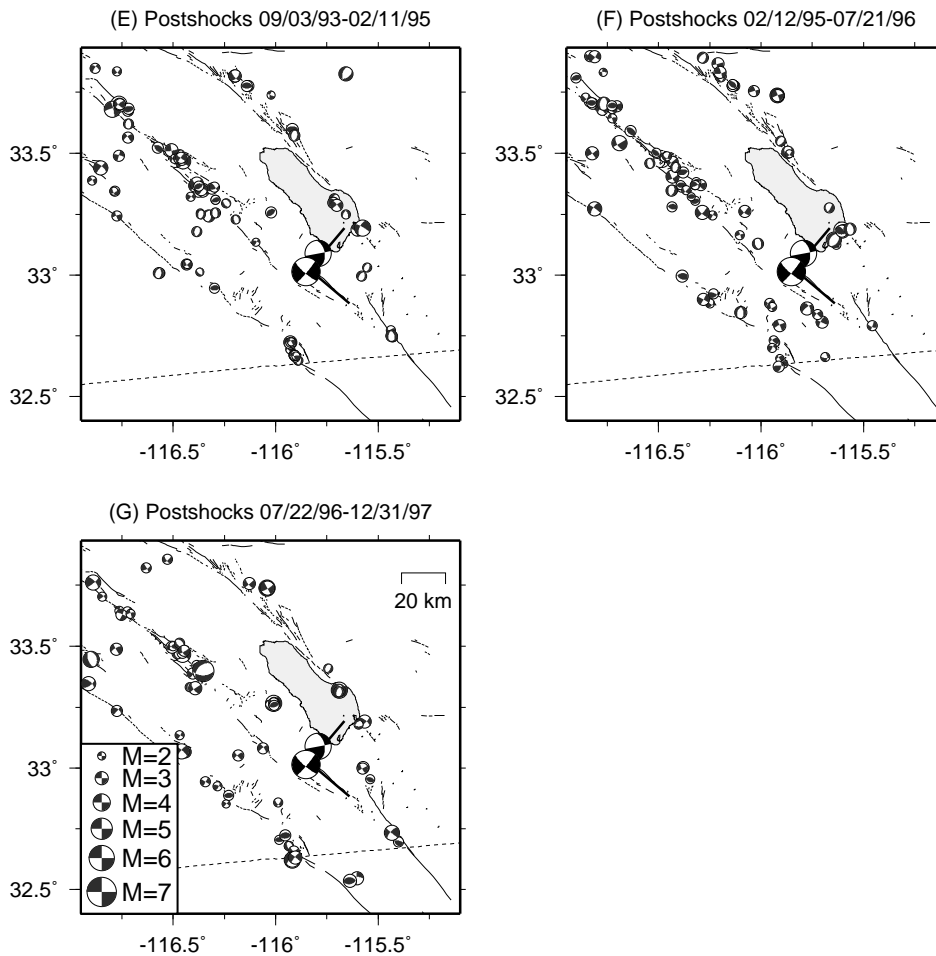


Figure 7. (continued)

changes.

Another, still more subtle, point is related to the desire to place time limits on the duration of possible triggering. The obvious way to do this is to bin the postshocks into non-overlapping time windows which are then compared to the preshock set. Those comparisons which result in a positive indication of triggering can then be given as the time range over which triggering is significant. Additionally, however, there will be fluctuations in the rate of seismicity which are again unrelated to the mainshock. Our only estimate of such fluctuations comes from the preshock set, and thus the preshocks must contain a sufficient number of events to give reliable estimates of not only the rate of background seismicity but also the temporal variability of that rate. Only by doing so can we determine which positive results are truly significant and which are merely chance.

Infinitely many fault plane slip models can be estimated which adequately explain the seismic and geodetic observations from a given mainshock. Each of these

models will lead to a different coseismic static stress field prediction, which will in turn lead to different results for any test of triggering. Some workers have attempted to quantify this effect by choosing a few different mainshock slip models for a particular event and examining the difference in the test results [e.g., *Reasen-berg and Simpson, 1992, 1997*]. However, another alternative which to our knowledge has not yet been addressed would be to examine extremal mainshock slip models [e.g., *Johnson et al., 1994*] which could give absolute bounds on the range of possible results from a particular test of triggering for a particular earthquake; this approach could be an important avenue for future work to explore.

Finally, in selecting a set of preshocks and postshocks for a given earthquake sequence we necessarily make choices as to which events will be included: magnitude, depth, distance, and time ranges; maximum location errors; and if the given test requires focal mechanism information, errors in focal mechanism parameters. All of this raises two additional issues: first is the question

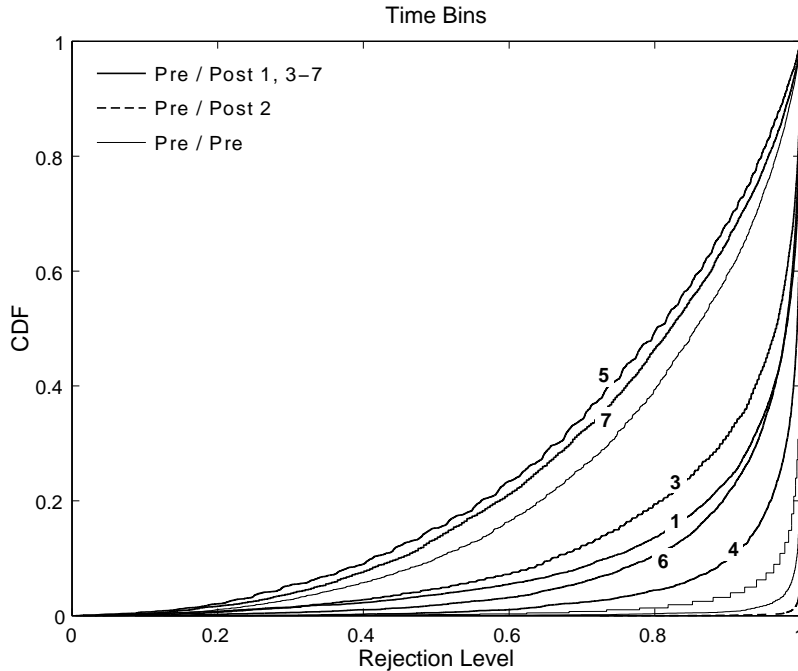


**Figure 8.** Results of applying the SD test to all ERSB events, with the preshocks and postshocks subdivided into 1.4-year bins. Thick lines are the CDF estimates for  $P_{KS}^{obs}$  values computed by comparing the first, third, fourth, fifth, sixth, and seventh bins of the postshocks to the entire set of preshocks using the SD test (individual curves are labeled with the bin number). Dashed line is the  $P_{KS}^{obs}$  CDF estimate for the second bin of postshocks (curve is not numbered). Thin lines are  $P_{KS}^{ref}$  estimates from Figure 6. Note that all  $P_{KS}^{obs}$  CDFs lie within the  $P_{KS}^{ref}$  range except for the  $P_{KS}^{obs}$  CDF for the second time bin.

of how these choices affect the final outcome of a given test, and second is how the errors in various parameters affect the computation of the static stress changes, and eventually the test results. While these issues may not be of primary importance, they should be considered in future tests for static stress triggering.

## 8. Summary

We have developed a new method to quantitatively test for the existence of static stress triggering following a large earthquake. Our method uses the Coulomb model of failure with event focal mechanism information and an assumed mainshock slip distribution to calculate static stress changes on the slip planes of events which occur both before and after the mainshock. We apply a bootstrap technique to resample our stress change data to account for the ambiguity in choosing the correct focal mechanism nodal plane (when  $\mu' \neq 0$ ) and possible biases resulting from our particular event selection. We then compute the statistical distributions of stress change values from several thousand bootstrap event resamplings and compare the distributions from events before and after the mainshock using the Kolmogorov-Smirnov test. From this comparison we derive estimates of the confidence with which we can reject the hypoth-

esis that the pre-mainshock and post-mainshock distributions are the same, which we convert to our confidence that the post-mainshock data are consistent (or not) with static stress triggering.

We have applied our test to the November 24, 1987, Elmore Ranch/Superstition Hills earthquake sequence in southern California. We use 14.2 years of data spanning the mainshock occurrence and find no evidence for significant static stress triggering when the events in our data set are taken as a whole. However, when we subdivide our data in time, we find significant triggering during the interval from 1.4 to 2.8 years following the mainshocks; we have no adequate explanation as to why significant triggering is not found earlier in the post-mainshock data. We also find significant triggering for events which experienced greater than about 0.01–0.03 MPa (0.1–0.3 bar) of applied coseismic Coulomb stress.

From our experience with this method we draw some general conclusions about tests for static stress triggering. Any test which uses focal mechanism information must be designed to handle the fundamental ambiguity in choosing which focal plane best matches the fault place that actually slipped, which can be done either with a priori information or through statistical means.

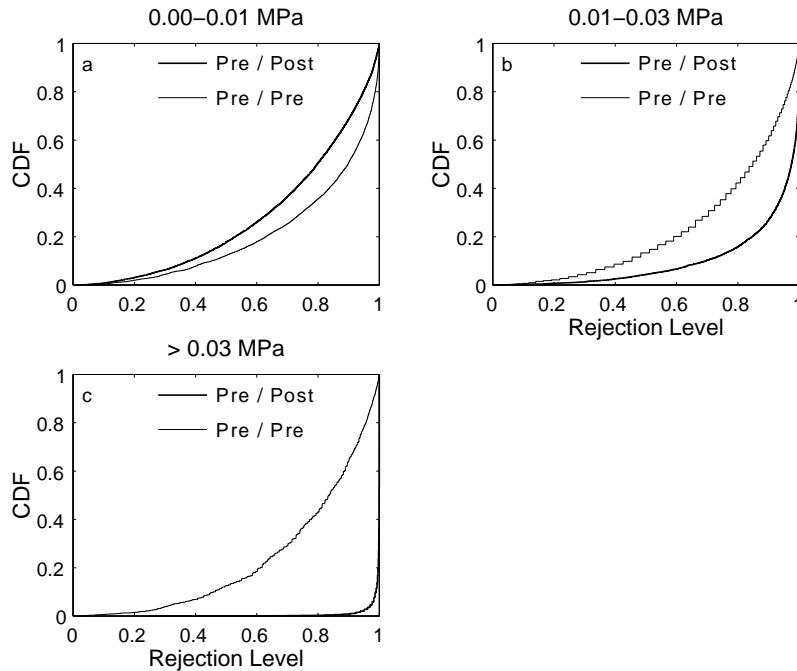


**Figure 9.** Results of applying the SD test to all ERSB events, with the events subdivided into three bins by applied stress magnitude. (a) Thick line is CDF of  $P_{KS}^{obs}$  values for preshocks/postshocks in the bin from 0 to 0.01 MPa applied stress change. Thin line is the CDF of  $P_{KS}^{ref}$  values for a single random half division of preshocks/preshocks (other random half divisions result in equivalent curves). (b) Same as Figure 9a, except stress bin runs 0.01 to 0.03 MPa. (c) Same as Figure 9a, except stress bin contains events which had induced stress of 0.03 MPa and higher. Note that in the last two bins the solid curve is shifted toward higher rejection level than is the dashed curve. Though not shown, the bootstrap CDF envelopes for the preshock/postshock comparisons for these two bins are also shifted toward higher NCFE than is the preshock/preshock bootstrap CDF envelope.

Also, the data set must contain sufficient events over as long a period of time as possible in order for meaningful conclusions to be drawn. More importantly, the reference set to which one compares the post-mainshock data must be large enough to give reliable estimates of both the behavior of background seismicity (above which stress triggering exists as a secondary effect) and the variability of that background behavior. Without this information, one cannot determine which effects seen in a given set of post-mainshock events are real evidence for static stress triggering and which are merely chance occurrences.

## Appendix: Kolmogorov-Smirnov Test

Our test depends on using the Kolmogorov-Smirnov (KS) statistical test [Press *et al.*, 1992], which may not be widely known, so we briefly discuss that technique here. The KS test is used in one of two ways. First, if one has a set of data and wants to know if they were drawn from a known statistical distribution (e.g., “are the data Gaussian distributed?”), the KS test can be used to give the probability with which this hypothesis can be rejected. More generally, in a situation where

one has two data sets and wants to know if the two were drawn from the same (unknown) underlying statistical distribution, the KS test can be used to estimate the probability with which one can reject the hypothesis that the data are in fact drawn from the same distribution. We apply the KS test in the second fashion.

Figure A1 demonstrates our use of the KS test. In this synthetic case, we know the underlying statistical distributions for the two data sets, shown as Gaussian probability density functions (PDFs)  $P_1$  and  $P_2$  in Figure A1a; clearly, the two distributions are different. However, assume we do not know the PDFs, and that we start with only the random data samples  $S_1$  and  $S_2$  shown in Figures A1b and A1c. Can we determine if these two data samples are drawn from the same distribution?

Figure A1d shows empirical cumulative distribution functions (CDFs)  $C_1$  and  $C_2$  computed from  $S_1$  and  $S_2$  as follows:

$$C(x) = \begin{cases} 0 & , \quad -\infty \leq x < x_1 \\ \frac{i}{N} & , \quad x_i \leq x < x_{i+1} \\ 1 & , \quad x_N \leq x \leq \infty \end{cases} \quad (A1)$$

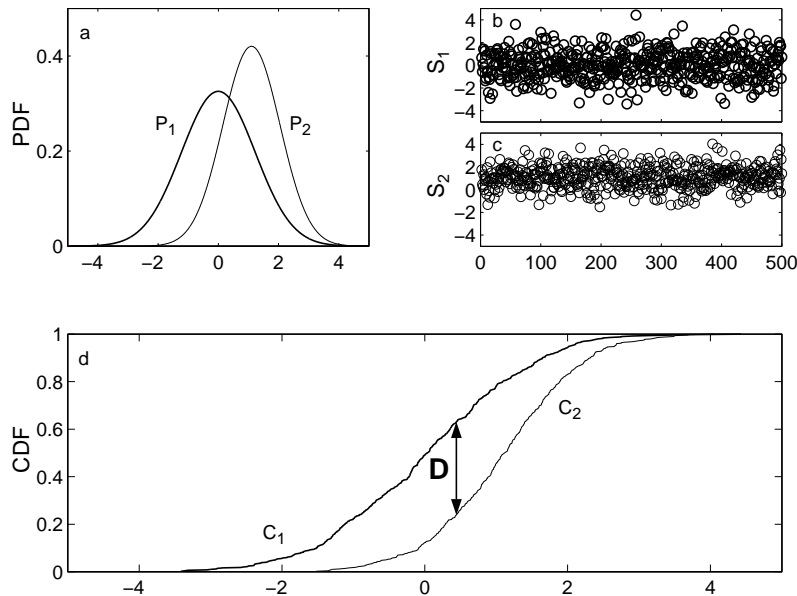


**Figure A1.** Synthetic Kolmogorov-Smirnov (KS) test example. (a) Underlying statistical distributions for data, represented as probability density functions (PDFs)  $P_1$  (thick line) and  $P_2$  (thin line). Curve notation is the same in all subfigures. (b) Random data sample  $S_1$  drawn on  $P_1$ . (c) Random data sample  $S_2$  drawn on  $P_2$ . (d) Empirical distribution functions  $C_1$  and  $C_2$ , derived from  $S_1$  and  $S_2$ . Line with arrows represents the KS test statistic  $D$  (see text).

where  $i = 1, 2, \dots, N-1$  and  $x_1, x_2, \dots, x_N$  are the values of the data series sorted into ascending order. The KS test statistic, shown as  $D$  in Figure A1d, is defined as the maximum absolute vertical deviation between  $C_1$  and  $C_2$ , or

$$D = \max_{-\infty < x < \infty} |C_1(x) - C_2(x)|, \quad (\text{A2})$$

and has a known (approximate) statistical distribution under the null hypothesis that the two data sets are drawn on the same distribution.

The confidence with which we can reject the null hypothesis that the two data sets are samples drawn from the same underlying distribution,  $P_{\text{KS}}$ , is given by

$$P_{\text{KS}}(\lambda) = 1 - Q_{\text{KS}}(\lambda). \quad (\text{A3})$$

$Q_{\text{KS}}(\lambda)$  can be computed to a good approximation as [Press *et al.*, 1992, pp. 624–625, equations 14.3.7, 14.3.9, 14.3.10]

$$Q_{\text{KS}}(\lambda) = 2 \sum_{k=1}^{\infty} (-1)^{k-1} e^{-2k^2\lambda^2}, \quad (\text{A4})$$

where

$$\lambda = \left( \sqrt{N_e} + 0.12 + \frac{0.11}{\sqrt{N_e}} \right) D, \quad (\text{A5})$$

$$N_e = \frac{N_1 N_2}{N_1 + N_2}, \quad (\text{A6})$$

and  $N_1$  and  $N_2$  are the number of values in  $S_1$  and  $S_2$ , respectively.

By this definition, large values of  $P_{\text{KS}}$  correspond to a high degree of confidence in rejecting the null hypothesis, so that, for example,  $P_{\text{KS}} = 0.95$  indicates that we can reject the null hypothesis at the 95% level. In the example shown in Figure A1,  $Q_{\text{KS}} = 5.5 \times 10^{-34}$ , giving  $P_{\text{KS}}$  essentially 1, and thus we can reject the hypothesis that  $S_1$  and  $S_2$  are drawn on the same distribution with practically 100% confidence.

One other point is worthy of note. The KS test only gives us a quantitative estimate of the confidence with which we can reject the hypothesis that two data sets are drawn from the same distribution. When used as we do in the SD test, the KS test does not give us any estimate of what that distribution might be.

**Acknowledgments.** Duncan Agnew and Cathy Constable made several useful suggestions on statistical techniques. Duncan Agnew, Steven Constable, Susanna Gross, Megan Flanagan, Ruth Harris, Shawn Larsen, Robert Simpson, and Frank Wyatt provided critical reviews of this manuscript. Shawn Larsen also answered with remarkable speed several questions regarding his slip distribution models. David Wald provides a great service on the World Wide Web for downloading those models (and others). This work makes use of event locations computed by and waveforms recorded by the Southern California Seismic Network (SCSN), which is operated jointly by the Seismological Laboratory at Caltech and the U.S. Geological

Survey, Pasadena. This research was supported by the Southern California Earthquake Center. SCEC is funded by NSF Cooperative Agreement EAR-8920136 and USGS Cooperative Agreements 14-08-0001-A0899 and 1434-HQ-97AG01718. SCEC contribution 448.

## References

- Anderson, J. G., J. N. Brune, J. N. Louie, Y. Zeng, M. Savage, G. Yu, Q. Chen, and D. dePolo, Seismicity in the western Great Basin apparently triggered by the Landers, California, earthquake, 28 June 1992, *Bull. Seismol. Soc. Am.*, *84*, 863–891, 1994.
- Beroza, G. C., and M. D. Zoback, Mechanism diversity of the Loma Prieta aftershocks and the mechanics of mainshock-aftershock interaction, *Science*, *259*, 210–213, 1993.
- Caskey, S. J., and S. G. Wesnousky, Static stress change and earthquake triggering during the 1954 Fairview Peak and Dixie Valley earthquakes, central Nevada, *Bull. Seismol. Soc. Am.*, *87*, 521–527, 1997.
- Efron, B., *The Jackknife, the Bootstrap, and Other Resampling Plans*, Soc. for Ind. and Appl. Math., Philadelphia, Penn., 1982.
- Efron, B., and R. Tibshirani, Bootstrap methods for standard errors, confidence intervals, and other measures of statistical accuracy, *Stat. Sci.*, *1*, 54–77, 1986.
- Erickson, L. L., A three-dimensional dislocation program with applications to faulting in the earth, Master's thesis, Stanford Univ., Palo Alto, Calif., 1986.
- Gomberg, J., and P. Bodin, Triggering of the  $M_S = 5.4$  Little Skull Mountain, Nevada, earthquake with dynamic strains, *Bull. Seismol. Soc. Am.*, *84*, 844–853, 1994.
- Gross, S. J., and C. Kisslinger, Stress and the spatial distribution of seismicity in the central Aleutians, *J. Geophys. Res.*, *99*, 15,291–15,303, 1994.
- Hanks, T. C., and C. R. Allen, The Elmore Ranch and Superstition Hills earthquakes of 24 November 1987: Introduction to the special issue, *Bull. Seismol. Soc. Am.*, *79*, 231–238, 1989.
- Hardebeck, J. L., J. J. Nazareth, and E. Hauksson, The static stress change triggering model: Constraints from two southern California aftershock sequences, *J. Geophys. Res.*, *103*, 24,427–24,437, 1998.
- Harris, R. A., Introduction to special section: Stress triggers, stress shadows, and implications for seismic hazard, *J. Geophys. Res.*, *103*, 24,347–24,358, 1998.
- Harris, R. A., and R. W. Simpson, Changes in static stress on southern California faults after the 1992 Landers earthquake, *Nature*, *360*, 251–254, 1992.
- Hill, D. P., et al., Seismicity remotely triggered by the magnitude 7.3 Landers, California, earthquake, *Science*, *260*, 1617–1623, 1993.
- Hodgkinson, K. M., R. S. Stein, and G. C. P. King, The 1954 Rainbow Mountain-Fairview Peak-Dixie Valley earthquakes: A triggered normal faulting sequence, *J. Geophys. Res.*, *101*, 25,459–25,471, 1996.
- Hudnut, K. W., L. Seeber, and J. Pacheco, Cross-fault triggering in the November 1987 Superstition Hills earthquake sequence, southern California, *Geophys. Res. Lett.*, *16*, 199–202, 1989.
- Jaeger, J. C., and N. G. W. Cook, *Fundamentals of Rock Mechanics*, 3 ed., Chapman and Hall, New York, 1979.
- Johnson, H. O., D. C. Agnew, and K. Hudnut, Extremal bounds on earthquake movement from geodetic data: Application to the Landers earthquake, *Bull. Seismol. Soc. Am.*, *84*, 660–668, 1994.
- Kilb, D., M. Ellis, J. Gomberg, and S. Davis, On the origin of diverse aftershock mechanisms following the 1989 Loma Prieta earthquake, *Geophys. J. Int.*, *128*, 557–570, 1997.
- King, G. C. P., R. S. Stein, and J. Lin, Static stress changes and the triggering of earthquakes, *Bull. Seismol. Soc. Am.*, *84*, 935–953, 1994.
- Larsen, S., R. Reilinger, H. Neugebauer, and W. Strange, Global Positioning System measurements of deformation associated with the 1987 Superstition Hills earthquake: Evidence for conjugate faulting, *J. Geophys. Res.*, *97*, 4885–4902, 1992.
- Li, V. C., S. H. Seale, and T. Cao, Postseismic stress and pore pressure readjustment and aftershock distributions, *Tectonophysics*, *144*, 37–54, 1987.
- Noir, J., E. Jacques, S. Békri, P. M. Adler, P. Tapponnier, and G. C. P. King, Fluid flow triggered migration of events in the 1989 Dobi earthquake sequence of central Afar, *Geophys. Res. Lett.*, *24*, 2335–2338, 1997.
- Nur, A., and J. R. Booker, Aftershocks caused by pore fluid flow?, *Science*, *175*, 885–887, 1972.
- Okada, Y., Internal deformation due to shear and tensile faults in a half-space., *Bull. Seismol. Soc. Am.*, *82*, 1018–1040, 1992.
- Oppenheimer, D. H., P. A. Reasenber, and R. W. Simpson, Fault plane solutions for the 1984 Morgan Hill, California, earthquake sequences: Evidence for the state of stress on the Calaveras Fault, *J. Geophys. Res.*, *93*, 9007–9026, 1988.
- Press, W. H., S. A. Teukolsky, W. T. Vetterling, and B. P. Flannery, *Numerical Recipes in C*, second ed., Cambridge Univ. Press, New York, 1992.
- Reasenber, P. A., and D. Oppenheimer, FPFIT, FPLOT, and FPPAGE: FORTRAN computer programs for calculating and displaying earthquake fault-plane solutions, *U.S. Geol. Surv. Open File Rep. 85-739*, U.S. Geol. Surv., 1985.
- Reasenber, P. A., and R. W. Simpson, Response of regional seismicity to the static stress change produced by the Loma Prieta earthquake, *Science*, *255*, 1687–1690, 1992.
- Reasenber, P. A., and R. W. Simpson, Response of regional seismicity to the static stress change produced by the Loma Prieta earthquake, in *The Loma Prieta, California, Earthquake of October 17, 1989—Aftershocks and Postseismic Effects*, U.S. Geol. Surv. Prof. Pap., 1550-D, edited by P. A. Reasenber, pp. D49–D71, U.S. Geol. Surv., 1997.
- Rice, J. R., and M. P. Cleary, Some basic stress diffusion solutions for fluid-saturated elastic porous media with compressible constituents, *Rev. Geophys.*, *14*, 227–241, 1976.
- Roeloffs, E. A., Fault stability changes induced beneath a reservoir with cyclic variations in water level, *J. Geophys. Res.*, *93*, 2107–2124, 1988.
- Rybecki, K., Analysis of aftershocks on the basis of dislocation theory, *Phys. Earth Planet. Inter.*, *7*, 409–422, 1973.
- Scholz, C. H., *The Mechanics of Earthquakes and Faulting*, Cambridge Univ. Press, New York, 1990.

- Skempton, A. W., The pore-pressure coefficients A and B, *Géotechnique*, 4, 143–147, 1954.
- Stein, R. S., and M. Lisowski, The 1979 Homestead Valley earthquake sequence, California: Control of aftershocks and postseismic deformation, *J. Geophys. Res.*, 88, 6477–6490, 1983.
- Stein, R. S., G. C. P. King, and J. Lin, Changes in failure stress on the southern San Andreas Fault system caused by the 1992 magnitude=7.4 Landers earthquake, *Science*, 258, 1328–1332, 1992.
- Stein, R. S., G. C. P. King, and J. Lin, Stress triggering of the 1994  $M = 6.7$  Northridge, California, earthquake by its predecessors, *Science*, 265, 1432–1435, 1994.
- Stein, R. S., A. A. Barka, and J. H. Dieterich, Progressive failure on the North Anatolian Fault since 1939 by earthquake stress triggering, *Geophys. J. Int.*, 128, 594–604, 1997.
- Toda, S., R. S. Stein, P. A. Reasenber, J. H. Dieterich, and A. Yoshida, Stress transferred by the 1995  $M_W = 6.9$  Kobe, Japan, shock: Effect on aftershocks and future earthquake probabilities, *J. Geophys. Res.*, 103, 24,543–24,565, 1998.

---

G. Anderson and H. Johnson, Cecil H. and Ida M. Green Institute of Geophysics and Planetary Physics, University of California, San Diego, La Jolla CA 92093-0225.

(anderson@python.ucsd.edu, hjohnson@ucsd.edu)

Received December 22, 1998; revised May 17, 1999; accepted June 15, 1999.

---

This preprint was prepared with AGU’s L<sup>A</sup>T<sub>E</sub>X macros v5.01, with the extension package ‘AGU++’ by P. W. Daly, version 1.6b from 1999/08/19.